


# Radiosynthesis and whole-body distribution in mice of a $^{18}\text{F}$ -labeled azepino[4,3-*b*]indole-1-one derivative with multimodal activity for the treatment of Alzheimer's disease

Sang Hee Lee<sup>1</sup> | Rosa Purgatorio<sup>2</sup> | Francesco Samarelli<sup>2</sup> | Marco Catto<sup>2</sup> |  
Nunzio Denora<sup>2</sup> | Maria Grazia Morgese<sup>3</sup> | Paolo Tucci<sup>3</sup> | Luigia Trabace<sup>3</sup> |  
Hye Won Kim<sup>1</sup> | Hyun Soo Park<sup>1</sup> | Sang Eun Kim<sup>1,4</sup> | Byung Chul Lee<sup>1,4</sup> |  
Modesto de Candia<sup>2</sup>  | Cosimo D. Altomare<sup>2</sup>

<sup>1</sup>Department of Nuclear Medicine, Seoul National University Bundang Hospital, Seoul National University College of Medicine, Seongnam, Republic of Korea

<sup>2</sup>Department of Pharmacy-Pharmaceutical Sciences, University of Bari Aldo Moro, Bari, Italy

<sup>3</sup>Department of Clinical and Experimental Medicine, University of Foggia, Foggia, Italy

<sup>4</sup>Center for Nanomolecular Imaging and Innovative Drug Development, Advanced Institutes of Convergence Technology, Suwon, Republic of Korea

## Correspondence

Modesto de Candia, Department of Pharmacy-Pharmaceutical Sciences, University of Bari Aldo Moro, Via E. Orabona 4, 70125 Bari, Italy.  
Email: [modesto.decandia@uniba.it](mailto:modesto.decandia@uniba.it)

Byung Chul Lee, Department of Nuclear Medicine, Seoul National University Bundang Hospital, Seoul National University College of Medicine, Seongnam 13620, Republic of Korea.  
Email: [leebc@snu.ac.kr](mailto:leebc@snu.ac.kr)

## Funding information

National Research Foundation of Korea (NRF), Grant/Award Number: (MEST) (2021R1A2C2003301); Program of Regione Puglia "Research for Innovation REFIN", Grant/Award Number: (POR PUGLIA FESR-FSE 2014/2020); Italian Ministry of Education, Universities and Research, Grant/Award Number: (PRIN, Grant 201744BN5T\_004)

## Abstract

Recently, the azepino[4,3-*b*]indole-1-one derivative **1** showed in vitro nanomolar inhibition against butyrylcholinesterase (BChE), the ChE isoform that plays a role in the progression and pathophysiology of Alzheimer's disease (AD), and protects against *N*-methyl-*D*-aspartate-induced neuronal toxicity. Three 9-*R*-substituted (*R* = F, Br, OMe) congeners were investigated. The 9-*F* derivative (**2a**) was found more potent as BChE inhibitors (half-maximal inhibitory concentration value = 21 nM) than **2b** (9-*Br*) and **2c** (9-*OMe*), achieving a residence time (38 s), assessed by surface plasmon resonance, threefold higher than that of **1**. To progress in featuring the in vivo pharmacological characterization of **2a**, herein the  $^{18}\text{F}$ -labeled congener **2a** was synthesized, by applying the aromatic  $^{18}\text{F}$ -fluorination method, and its whole-body distribution in healthy mice, including brain penetration, was evaluated through positron emission tomography imaging. [ $^{18}\text{F}$ ]**2a** exhibited a rapid and high brain uptake ( $3.35 \pm 0.26\% \text{ ID g}^{-1}$  at  $0.95 \pm 0.15$  min after injection), followed by a rapid clearance ( $t_{1/2} = 6.50 \pm 0.93$  min), showing good blood-brain barrier crossing. After a transient liver accumulation of [ $^{18}\text{F}$ ]**2a**, the intestinal and urinary excretion was quantified. Finally, ex vivo pharmacological experiments in mice showed that the unlabeled **2a** affects the transmitters' neurochemistry, which might be favorable to reverse cognition impairment in mild-to-moderate AD-related dementias.

## KEYWORDS

$^{18}\text{F}$ -labeling, butyrylcholinesterase inhibitor, in vivo distribution, neurochemistry, positron emission tomography

Sang Hee Lee and Rosa Purgatorio contributed equally to this study.

This is an open access article under the terms of the [Creative Commons Attribution](https://creativecommons.org/licenses/by/4.0/) License, which permits use, distribution and reproduction in any medium, provided the original work is properly cited.

© 2023 The Authors. *Archiv der Pharmazie* published by Wiley-VCH GmbH on behalf of Deutsche Pharmazeutische Gesellschaft.

## 1 | INTRODUCTION

Alzheimer's disease (AD) is a chronic neurodegenerative disorder, accounting for most elderly-related dementias. Recent World Alzheimer Reports predicted that people affected by AD will increase to more than 131 million by 2050.<sup>[1]</sup> The main histopathological hallmarks of AD are the generation and deposition of senile plaques, incorporating the extracellular neurotoxic amyloid- $\beta$  (A $\beta$ ) peptide aggregates, along with intracellular neurofibrillary tangles of hyperphosphorylated  $\tau$ -protein, which triggers oxidative stress, perturbation of cellular metabolism, and finally synaptic and neuronal loss,<sup>[2]</sup> and the impairment of the cholinergic neurotransmission.<sup>[3]</sup>

Albeit the advances in understanding the multifactorial nature of AD, including the epigenetic mechanisms underlying the disease,<sup>[4]</sup> efforts to develop disease-modifying agents failed, and the available treatments only address the symptoms of mild-to-moderate AD. The approved drugs include three acetylcholinesterase (AChE) inhibitors (rivastigmine, galantamine, and donepezil [DNPZ]) and one *N*-methyl-D-aspartate receptor (NMDAR) antagonist (memantine) to counteract decreased acetylcholine (ACh) level and glutamate-induced excitotoxicity in AD brain, respectively.<sup>[5]</sup> The cholinergic system is a network of neurons, glia, and immune cells that use the excitatory neurotransmitter ACh in physiological processes.<sup>[6]</sup> In the central nervous system (CNS), namely, in the neocortex and hippocampus (HIPP), neurochemical changes due to imbalance of ACh synthesis/degradation equilibrium constitute a major causal factor of disorders in learning, memory, behavior, and emotional responses.<sup>[7–10]</sup>

ACh levels and cholinergic transmission in the brain are regulated by the two enzyme isoforms, namely, AChE hydrolyzing ACh in the synaptic cleft of the cholinergic neurons and butyrylcholinesterase (BChE), but at higher ACh concentrations.<sup>[11,12]</sup> ChEs' inhibition has been widely associated with cognitive and persistent benefits over time in AD, with reduced mortality risk.<sup>[13]</sup> BChE is associated with the CNS glial cells, vascular structures, and neurons, where it may serve as a coregulator of the cholinergic neurotransmission. BChE is primarily located in the CNS amygdala, HIPP, and thalamus, which are involved in cognition and behavior functions compromised in AD.

Despite BChE activity is normally observed at higher levels in the white matter and CNS glial cells, in both animal models and postmortem brain samples of AD patients, an increase of BChE expression and activity has been observed<sup>[14]</sup> in association with A $\beta$ -amyloid plaques and neurofibrillary tangles. Data from animal models would suggest an active role of BChE in the pathogenesis of AD, leading to consider BChE as a pharmacological (co)target, and/or a diagnostic marker of disease progression, and the BChE inhibitors (BChE-Is) are worthy of consideration as anti-AD pharmacological agents.<sup>[11,12]</sup> Interestingly, due to the lack of peripheral side effects (i.e., gastrointestinal, cramps), BChE-Is may be more tolerated than the AChE inhibitors.

We recently reported indole-fused medium-sized azaheterocycles, achieving good ChE inhibition activity and high BChE selectivity.<sup>[15]</sup> The 2,3,4,5-tetrahydroazepino[4,3-*b*]indole-1(2*H*)-one (THAI) moiety was identified as a scaffold (structurally related to the well-known carbazoles

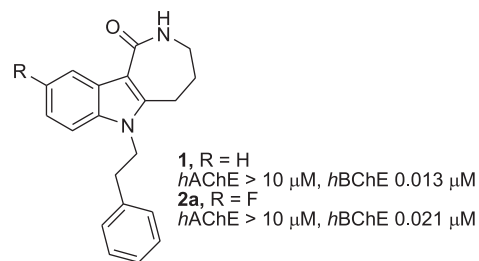


**FIGURE 1** Structures of two recently reported 2,3,4,5-tetrahydroazepino[4,3-*b*]indol-1(2*H*)-one derivatives (**1** and **2a**) as butyrylcholinesterase (BChE)-selective inhibitors. AChE, acetylcholinesterase.

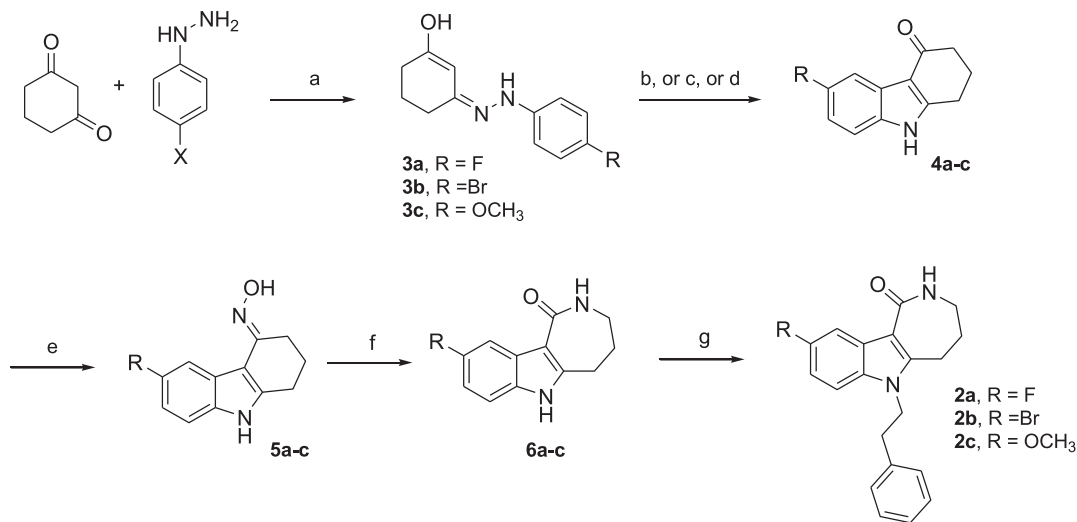
and carbolines) of novel multitarget-directed ligands (MTDLs) addressing some key pathogenic pathways underlying AD.<sup>[16–18]</sup> Among them, the 6-phenethyl-THAI derivative **1** (Figure 1) achieved low nanomolar BChE inhibition potency, and the 9-F congener **2a** was found equipotent to **1**. In addition to BChE-selective inhibition, THAI derivatives showed protective effects against *N*-methyl-D-aspartate (NMDA)-induced excitotoxicity on neuronal SH-SY5Y cells.

Considering the *in vitro* biological profile, the low cytotoxicity, and the predicted good blood-brain barrier (BBB) crossing, to progress in featuring the *in vivo* pharmacological profile of **2a**, we conducted a preliminary evaluation of its whole-body distribution in mice by positron emission tomography (PET) imaging, synthesizing a THAI-labeled tracer. THAI **1** could be potentially labeled with radioisotopes (e.g., <sup>18</sup>F, <sup>76</sup>Br, or <sup>11</sup>C) from suitable precursors, and we prepared three unlabeled analogs (**2a–c**), bearing 9-F, 9-Br, and 9-OCH<sub>3</sub> substituents. The preliminary evaluation of the anti-ChE activities of **2a–c** guided the selection of the 9-F THAI congener (**2a**) that underwent the radiolabeling procedure. [<sup>18</sup>F]**2a** was synthesized and characterized, and its *in vivo* distribution in healthy mice was investigated. The effects of the intraperitoneally (i.p.) administered single dose (20 mg kg<sup>-1</sup>) of **2a** on different brain neurotransmitters involved in behavioral responses (i.e., serotonin [5-HT], dopamine [DA], noradrenaline [NA]) were studied in healthy mice through *ex vivo* neuropharmacological assays to forecast developments of **2a** as an anti-AD agent.

## 2 | RESULTS AND DISCUSSION

### 2.1 | Chemistry

Compounds **2a–c** were synthesized according to the reported procedures (Scheme 1).<sup>[16–18]</sup> Suitable 4-substituted phenyl hydrazines were reacted with 1,3-cyclohexanedione, providing the hydrazone intermediates (**3a–c**), which were converted to the corresponding 1,2,3,9-tetrahydro-4*H*-carbazol-4-ones (**4a–c**) under Fischer conditions. The 8-F carbazolone (**4a**) was synthesized by refluxing the F-substituted hydrazone derivative (**3a**) in the presence of trifluoroacetic acid (TFA) for 2 days.



**SCHEME 1** Reagents and conditions: (a) 4-Fluorophenylhydrazine hydrochloride, water, room temperature (r.t.), 15 h, 90%; 4-bromophenylhydrazine hydrochloride, water, r.t., overnight, 90%; 4-methoxyphenylhydrazine hydrochloride, Na<sub>2</sub>CO<sub>3</sub>, water, r.t., overnight, 90%; (b) trifluoroacetic acid, reflux, 48 h, 50%–65%; (c) H<sub>2</sub>SO<sub>4</sub>/H<sub>2</sub>O (1:2 v/v), 80°C, 2 h, 70%; (d) *p*-TsOH, *n*-BuOH, 100°C, 1 h, 60%; (e) NH<sub>2</sub>OH × HCl, AcONa, EtOH/water (2:1 v/v), reflux, 24 h, 60%; (f) preheated polyphosphoric acid (90–110°C), 30 min, 45%–90%; (g) 2-phenylethyl bromide, tetrabutyl ammonium bromide, 25% NaOH/methylene chloride (1:2 v/v), r.t., 48 h, 45%–61%.

The 8-Br carbazolone (**4b**) was synthesized by treating the Br-substituted hydrazone (**3b**) for 2 h in a degassed and 80°C preheated H<sub>2</sub>SO<sub>4</sub>/H<sub>2</sub>O (1:2 v/v) mixture. The same conditions applied to the synthesis of the 8-OCH<sub>3</sub> carbazolone (**4c**) resulted in poorer yields. On the contrary, the intermediate **4c** was obtained in satisfactory yields by heating the hydrazone derivative (**3c**) in *n*-BuOH at 100°C, along with equimolar amount of *p*-TsOH. Conversion of carbazolones into ketoximes (**5a–c**), and the regioselective Beckmann rearrangement in preheated polyphosphoric acid (PPA), changing the reaction temperature to 90–110°C, provided the substituted THAI products (**6a–c**) in good yields (>70%). Finally, a selective alkylation to introduce the phenethyl group on the indole nitrogen (N<sub>5</sub>) underwent in NaOH methylene chloride biphasic mixtures, in the presence of tetrabutyl ammonium bromide (TBAB) as the phase transfer catalyst to afford the three 9-substituted 2,3,4,5-tetrahydroazepino[4,3-*b*]indol-1(2*H*)-one derivatives (**2a–c**).

## 2.2 | In vitro biological characterization of 9-substituted THAI derivatives

By applying the Ellman colorimetric assay, according to a previously reported protocol,<sup>[18,19]</sup> and using DNPZ and tacrine (TAC) as positive controls, the in vitro inhibitory activities of **1** and the 9-*X*-substituted analogs **2a–c** were determined toward heterologous cholinesterases (electric eel [ee] AChE and horse serum [hs] BChE), and the human ChE isoforms. The values, expressed as the half-maximal inhibitory concentration values (IC<sub>50</sub>) or inhibition percentage at the maximum concentration tested (25 μM), are summarized in Table 1.

The THAI derivatives **1** and **2a** confirmed to be almost equipotent as BChE-Is in the low nanomolar range of concentrations.<sup>[16]</sup> While no

appreciable difference emerged between the inhibition data toward the species-related ChEs' isoforms, bulkiness of the R substituent at position 9 should affect the BChE inhibition potency. In fact, Br (**2b**) and OMe (**2c**), bulkier than F, resulted in congeners 10- and fivefold less potent than **2a**, respectively.

The binding kinetics and affinity of **1** and **2a** toward BChE was further featured by using a surface plasmon resonance (SPR) biosensor (Figure S1 in Supporting Information). The hs BChE, which shares high homology with the human isoform but higher stability, was first immobilized on a COOH-V sensor chip surface by amine coupling, resulting in an efficient biosensor, even after repeated regeneration cycles with a 3 M NaCl solution (details on protocols for immobilization and assay in the experimental section).<sup>[17]</sup> Briefly, assay solutions of tested compounds were prepared by dissolving 10 mM dimethyl sulfoxide (DMSO) solutions in 10 mM phosphate buffer (PB) (pH 8) up to a final 2% DMSO concentration, as matched in the running buffer. The assay solutions were injected over BChE functionalized surface, avoiding any limitation by mass transfer, and after completion of injection, the running buffer was flowed to allow a complete dissociation phase, without regeneration cycles. The results obtained with good approximation are summarized in Table 2.

The K<sub>D</sub> values of **1** and **2a**, along with the reference drugs TAC and DNPZ, agreed with the inhibition potency (IC<sub>50</sub>) data. The binding curves (Figure S1 in Supporting Information) rapidly reached the response at equilibrium for **1**, TAC and DNPZ, which appeared as fast and reversible BChE binders. Compounds **1** and **2a** showed close BChE affinities, the main difference lying in the association (*k*<sub>on</sub>) and dissociation rate constants (*k*<sub>off</sub>). Compared to **1**, **2a** showed one order of magnitude lower association rate (*k*<sub>on</sub>), and about four times slower dissociation rate (*k*<sub>off</sub>) values, which

**TABLE 1** Inhibitory activities on cholinesterases of 9-X-substituted 2,3,4,5-tetrahydroazepino[4,3-*b*]indol-1(2*H*)-one derivatives.

Compound	AChE IC <sub>50</sub> (μM) <sup>a</sup>		BChE IC <sub>50</sub> (μM) <sup>a</sup>	
	Electric eel	Human	Equine	human
<b>1</b> <sup>b</sup>	20.0 ± 2.0	18.9 ± 1.6	0.024 ± 0.004	0.013 ± 0.002
<b>2a</b> <sup>b</sup>	[17 ± 7%]	[9 ± 5%]	0.028 ± 0.002	0.021 ± 0.003
<b>2b</b>	[21 ± 3%]	[26 ± 8%]	1.90 ± 0.09	2.10 ± 0.12
<b>2c</b>	[32 ± 6%]	[34 ± 8%]	0.140 ± 0.074	0.125 ± 0.050
TAC <sup>c</sup>	0.30 ± 0.05	0.53 ± 0.01	0.025 ± 0.002	0.020 ± 0.011
DNPZ <sup>c</sup>	0.021 ± 0.002	[0.010 ± 0.005]	2.30 ± 0.12	1.95 ± 0.12

Abbreviations: AChE, acetylcholinesterase; DNPZ, donepezil; IC<sub>50</sub>, half-maximal inhibitory concentration value; TAC, Tacrine.

<sup>a</sup>IC<sub>50</sub> values determined by interpolation of the sigmoidal dose–response curves as obtained by regression with GraphPad Prism software (ver. 5.01) of at least seven data points, or percent inhibition at 10 μM concentration in square brackets for compounds achieving less than 40% inhibition at 25 μM; data are mean ± SD of three independent measurements.

<sup>b</sup>The previously reported compounds **1** and **2a**<sup>[16]</sup> were retested in this study.

<sup>c</sup>TAC and DNPZ were used as positive controls.

**TABLE 2** Affinity kinetics data to BChE, affinity to HSA and aqueous solubility of 9-*R*-substituted 2,3,4,5-tetrahydroazepino[4,3-*b*]indol-1(2*H*)-one derivatives.

Compound	BChE <sup>a</sup>				HSA <sup>b</sup>	
	K <sub>D</sub> (μM)	k <sub>on</sub> (M <sup>-1</sup> s <sup>-1</sup> )	k <sub>off</sub> (s <sup>-1</sup> )	τ (s)	K <sub>D</sub> (μM)	S (mM) <sup>c</sup>
<b>1</b>	0.0082 ± 0.006	1.00 × 10 <sup>7</sup>	0.08279	12	0.850 ± 0.012	0.174
<b>2a</b>	0.012 ± 0.003	2.30 × 10 <sup>6</sup>	0.02645	38	0.241 ± 0.028	0.038
TAC <sup>b</sup>	0.016 ± 0.003	1.92 × 10 <sup>7</sup>	0.0670	15		
DNPZ <sup>b</sup>	7.20 ± 0.20	1.40 × 10 <sup>9</sup>	0.13711	7		
Warfarin					5.50 ± 0.30	

Abbreviations: BChE, butyrylcholinesterase; DNPZ, donepezil; HSA, human serum albumin; PBS, phosphate-buffered saline; SPR, surface plasmon resonance; TAC, tacrine.

<sup>a</sup>Binding parameter to immobilized equine serum BChE as determined by SPR; TAC and DNPZ were used as positive controls. Data are means of at least three independent measurements; reported values: equilibrium dissociation constants (K<sub>D</sub>), association rate constants (k<sub>on</sub>), dissociation rate constants (k<sub>off</sub>), and residence time (τ).

<sup>b</sup>Binding to immobilized HSA, measured by SPR. Warfarin was reported as the reference, and its K<sub>D</sub> value resulted close to those previously reported.<sup>[18]</sup> Data are mean ± SD of at least three independent measurements.

<sup>c</sup>Aqueous solubility determined in 0.05 M PBS, pH 7.40 (0.15 M KCl) at 25 ± 1°C.

resulted in different half-lives of enzyme–ligand complex, as highlighted by the differences in residence times (12 and 38 s for **1** and **2a**, respectively).

The interactions of compounds **1** and **2a** and human serum albumin (HSA) were also determined by SPR. HSA represents the most abundant protein in plasma, playing a key role in modulating the ADME profiles of xenobiotics. The assessment of the binding affinity to HSA can help to estimate the bioavailability in the early stage of drug design and development. Compounds **1** and **2a** appeared as fast and reversible HSA binders, endowed with high affinity to the circulating protein. The higher affinity site of HSA was occupied at concentrations lower than 15 μM with a dissociation constant (K<sub>D</sub>) of 0.85 and 0.24 μM for compounds **1** and **2a**, respectively. Considering the physiological HSA concentration in plasma (680 μM), at 10 μM concentration, both compounds can be predicted bound to HSA for distribution to the peripheral tissues.

Applying the thermodynamic equilibrium method, the experimental aqueous solubility of compound **2a** was determined (Table 2 and Supporting Information Table S2). According to that predicted by SwissADME (3.80 × 10<sup>-2</sup> mM), the aqueous solubility of **2a** was almost five times lower than that of **1** (Table 2), but yet ranking it as a moderately water-soluble compound (6 < Log S < 2).

### 2.3 | Ex vivo neurochemical assays

Besides the cholinergic hypothesis, multiple neurotransmitter abnormalities can affect the AD brain, and some other related neurological disorders, which may benefit from drugs with multiple effects.<sup>[20]</sup> We investigated the ability of compound **2a** to affect brain neurotransmission in healthy mice, by quantitatively determining noradrenaline (NA), dopamine (DA), and serotonin (5-HT) content in the

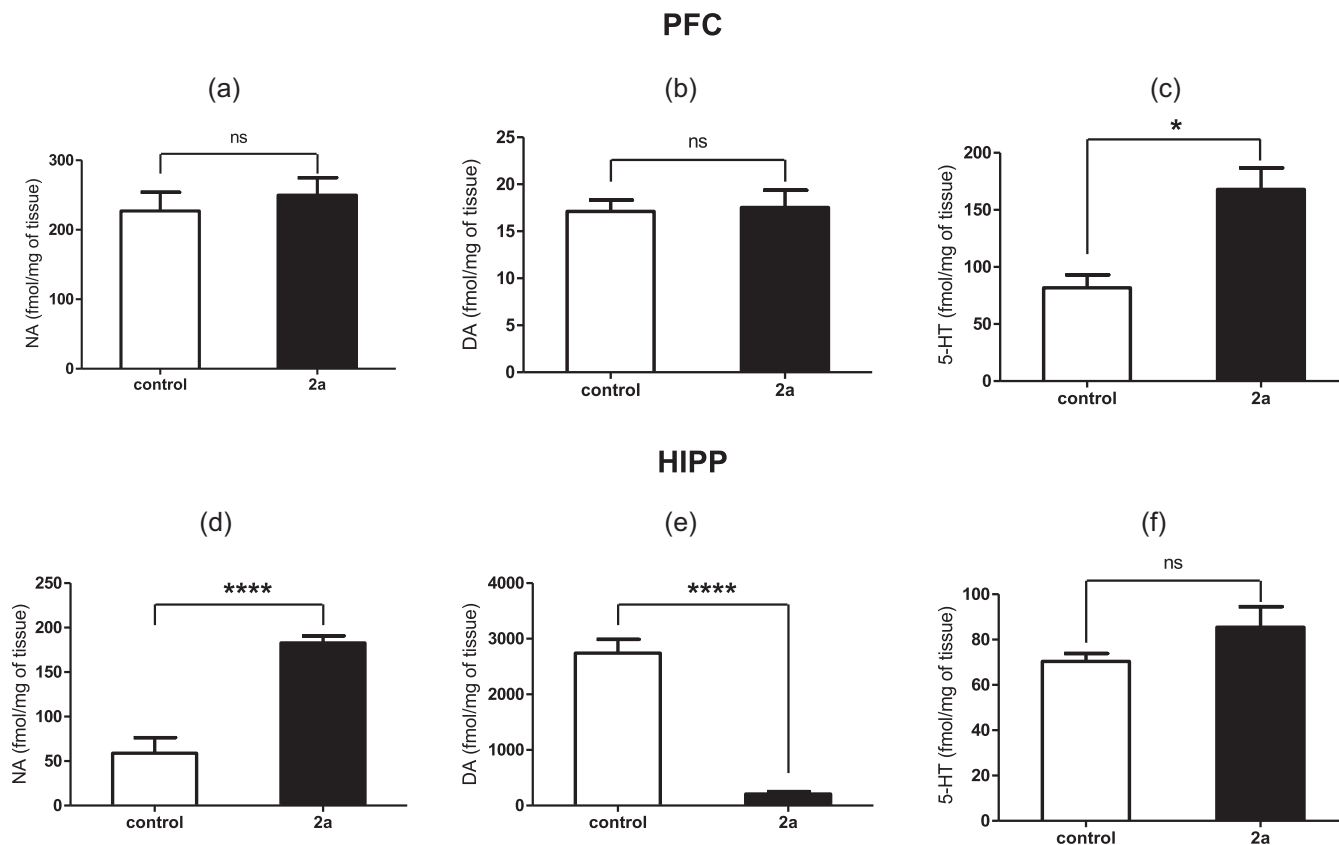


**FIGURE 2** Effect on monoamine content in the prefrontal cortex (PFC) and hippocampus (HIPP) of **2a**-treated mice ( $20 \text{ mg kg}^{-1}$  in  $10 \text{ mL}$  vehicle,  $n = 5$ ), and control mice ( $10 \text{ mL kg}^{-1}$ ,  $n = 4$ ), after intraperitoneal administration. (a) PFC content of noradrenaline (NA) ( $\text{fmol } \mu\text{L}^{-1}$ ); (b) PFC content of dopamine (DA) ( $\text{fmol } \mu\text{L}^{-1}$ ); (c) PFC content of serotonin (5-HT) ( $\text{fmol } \mu\text{L}^{-1}$ ); (d) HIPP content of NA ( $\text{fmol } \mu\text{L}^{-1}$ ); (e) HIPP content of DA ( $\text{fmol } \mu\text{L}^{-1}$ ); (f) HIPP content of 5-HT ( $\text{fmol } \mu\text{L}^{-1}$ ). n.s., not significant. Unpaired Student's *t* test: <sup>n.s.</sup> $p > 0.05$ , <sup>\*</sup> $p < 0.05$ , <sup>\*\*\*\*</sup> $p < 0.0001$ .

prefrontal cortex (PFC) and HIPP of mice treated with **2a**, at a dose of  $20 \text{ mg kg}^{-1}$  (or vehicle) i.p., 30 min after administration. The results are shown in Figure 2.

The quantification analysis of neurotransmitter distribution showed that NA and DA content in PFC brain area was not affected by administration of **2a** (Figures 2a,b), while 5-HT levels were significantly increased in **2a**-treated mice, in comparison to control (Figure 2c; unpaired Student's *t* test with Welch's correction). As for the HIPP area, after i.p. administration **2a** induced a significant increase in NA level (Figure 2d) and a significant reduction in DA content in this brain area (Figure 2e). Finally, significant alteration in hippocampal 5-HT concentration was not evidenced after administration (Figure 2f).

After i.p. administration, compound **2a** was, therefore, able to diversely alter PFC and HIPP neurochemistry. A significantly increased 5-HT content was determined in the cortical area, which could be particularly interesting considering that very often neuropsychiatric complications, such as depression, accompany or even precede neurological disorders. Therefore, the increase in cortical 5-HT may be beneficial, since drugs able to enhance serotonergic neurotransmission have been shown to facilitate A $\beta$  clearance,<sup>[21]</sup> and influence APP processing toward A $\beta$  production.<sup>[22,23]</sup>

Regarding the hippocampal area, NA level was also found to be significantly increased in **2a**-treated mice compared to control. Such an outcome is in line with previously reported increased NA release after the administration of AChE inhibitors.<sup>[24]</sup> This effect may result favorable in the AD treatment, as NA regulates cognitive and behavioral functions and can also protect neurons against a variety of insults that lead to inflammatory and oxidative unbalances,<sup>[25]</sup> such as the A $\beta$  production and a reduction in NA concentration often occurring in AD patients.<sup>[26]</sup> Considering the indication of NA as an endogenous suppressor of brain inflammatory responses,<sup>[27]</sup> drugs able to increase NA release, along with ACh release, may be advantageous.<sup>[28]</sup> As far as the dopaminergic system is concerned, we found DA concentrations were significantly decreased in HIPP after **2a** treatment. These results are in line with previous data indicating a reduction in DA levels after inhibition of AChE.<sup>[29]</sup> It is known that cholinergic and dopaminergic systems are interconnected and play a role in the modulation of memory processes. In good agreement, the DA system involved in cognitive functions and located in brain areas such as HIPP and cerebral cortex is under cholinergic control. In our experimental procedure, we recognized an area-dependent effect, and DA reduction was strongly evident only at hippocampal levels. This dramatic reduction in DA levels may be

secondary to nicotinic receptor desensitization occurring after AChE inhibition as shown for other areas such as the striatum.<sup>[30]</sup> It has been reported that the BChE distribution is involved in the coregulation of cholinergic and noncholinergic neurotransmission at the hippocampal level in humans; therefore, the area-specific effect retrieved might overlap BChE distribution and specific function in that area.<sup>[31]</sup>

Whole physicochemical and neurochemical data, as well as the recent interest devoted to identification of PET tracers based on competitive inhibitors to study the BChE role in AD progression,<sup>[32,33]</sup> prompted us to investigate the *in vivo* ability of **2a** to cross BBB and penetrate CNS, and its whole-body distribution. To do this, we undertook the radiosynthesis of [<sup>18</sup>F]**2a** to study the distribution into the brain and the peripheral organs in mice. The <sup>18</sup>F isotope, which has a half-life of 109.8 min, showed favorable properties over other radioisotopes commonly used for nuclear imaging techniques, high positron yields, and a good spatial resolution, which is a result of relatively low positron energies.<sup>[6]</sup>

## 2.4 | Radiosynthesis of <sup>18</sup>F-labeled compound **2a**

The <sup>18</sup>F-labeled **2a** was synthesized by direct aromatic <sup>18</sup>F-fluorination of the boron ester precursor,<sup>[29]</sup> preferred to hypervalent iodine<sup>[34]</sup> and stannyl compounds,<sup>[35]</sup> following a consolidated in-house developed method (Scheme 2).<sup>[34]</sup> The precursor **7** was prepared starting from the 9-Br analog **2b**.

The boronic acid pinacol ester precursor (**7**) was prepared from compound **2b** by a Suzuki–Miyaura borylation, in the presence of [1,1'-bis(diphenylphosphino)ferrocene]palladium(II) dichloride, bis(pinacolato)diboron and potassium acetate in dimethylformamide (DMF) at 80°C. [<sup>18</sup>F]**2a** was synthesized via a copper-mediated aromatic <sup>18</sup>F-fluorination in the presence of the precursor **7**, Cu(OTf)<sub>2</sub>, pyridine, and the dried 18-Crown-6/<sup>18</sup>F-Cs<sup>+</sup> complex in DMF, according to the previously described method.<sup>[20,21]</sup> After the reaction, [<sup>18</sup>F]**2a** was purified by semipreparative high-performance liquid chromatography (HPLC) system (Supporting Information, Figure S3) with 10 ± 5% of radiochemical yield (*n* = 8, decay corrected), high radiochemical purity (>99%), and high molar activity (126 ± 27 GBq μmol<sup>-1</sup>; Supporting Information, Figure S4). The identity of

[<sup>18</sup>F]**2a** was confirmed by coinjection with the authentic **2a** into the analytical HPLC column (Supporting Information, Figure S5).

## 2.5 | Stability and lipophilicity of [<sup>18</sup>F]**2a**

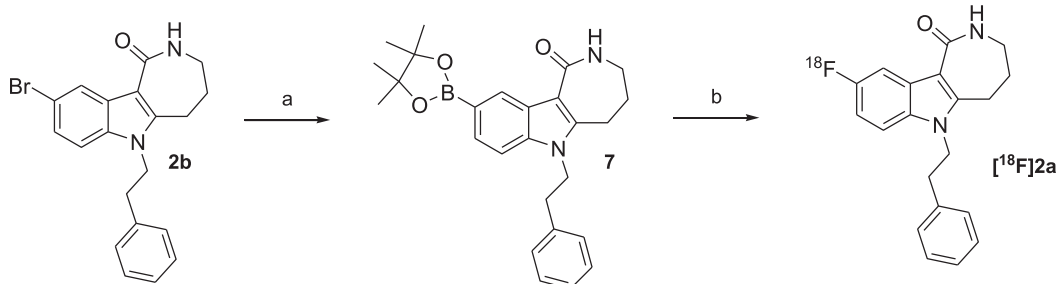
Radio-thin layer chromatography (radio-TLC) was applied to study the *in vitro* stability of the radioligand [<sup>18</sup>F]**2a** in human serum from healthy volunteers. The samples were incubated with human serum at 37°C, and aliquots were taken off at 0, 30, 60, 90, and 180 min, mixed with CH<sub>3</sub>CN, then centrifuged, and the resulting supernatants analyzed by a radio-TLC scanner. [<sup>18</sup>F]**2a** did not undergo any noticeable degradation, such as defluorination or any kind of breakdown, within 180 min after incubation in human plasma (Supporting Information, Figure S6).

Compound **2a** was predicted by admetSAR software<sup>[36]</sup> as a good brain-permeating compound (CNS+). The lipophilicity of [<sup>18</sup>F]**2a** was determined by the micro shake-flask method (Supporting Information, Table S7). The distribution coefficient between pH 7.4 aqueous phosphate-buffered saline (PBS) and *n*-octanol (Log *D*<sup>7.4</sup>) was found equal to 3.35 ± 0.04. The experimental Log *D* value falls within the range of 2.0–3.5, which is established as optimal to achieve high/good penetration across BBB and limit the target to nontarget ratios.<sup>[37]</sup>

## 2.6 | Whole-body distribution study of [<sup>18</sup>F]**2a** in healthy mice

The *in vivo* biodistribution study was assessed by intravenously administering a single dose of a solution of newly radiosynthesized compound [<sup>18</sup>F]**2a** in healthy ICR (Institute of Cancer Research) mice to provide a quantitative evaluation of biodistribution levels in brain tissues, organs, and whole body, by using a small animal PET/CT scanner system to obtain dynamic images and generate time-activity curves of regions of interest (Figure 3).

PET measurements of the whole radioactivity related to [<sup>18</sup>F]**2a** were performed in 0–90 min intervals. A suitable radiotracer for the brain should have a good penetration of the BBB, that is, a high uptake after intravenous bolus injection (2%–4% ID g<sup>-1</sup> in mice), low



**SCHEME 2** Reagents and conditions: (a) [1,1'-bis(Diphenylphosphino)ferrocene]palladium(II) dichloride, CH<sub>3</sub>CO<sub>2</sub>K, bis(pinacolato)diboron, dimethylformamide (DMF), 80°C, 5 h, argon gas, 31%; (b) [<sup>18</sup>F]fluoride, Cu(OTf)<sub>2</sub>, pyridine, 18-Crown-6, CsHCO<sub>3</sub>, DMF, 110°C, 10 min.

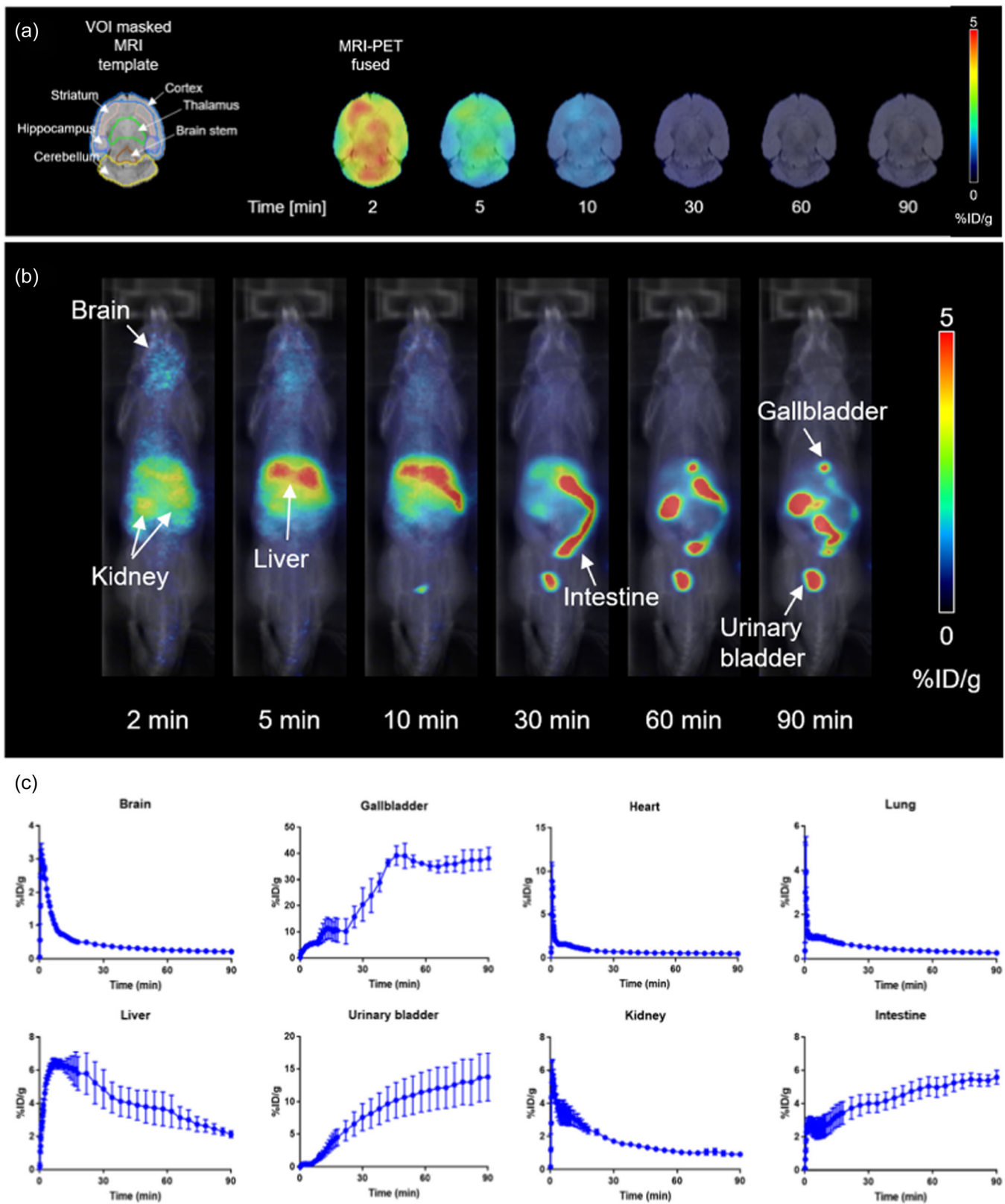


**FIGURE 3** Representative positron emission tomography images (a and b) and time-activity curves (c) of  $[^{18}\text{F}]2\text{a}$  in the brain, gallbladder, heart, lungs, liver, urinary bladder, kidneys, liver, and intestine in the healthy mice. The results are expressed as mean  $\pm$  SD,  $n = 3$ .

**TABLE 3** PET-based assessment of in vivo distribution of [<sup>18</sup>F]2a.

	$T_{\max}$ (min)	$C_{\max}$ (%ID g <sup>-1</sup> )	AUC (% ID g <sup>-1</sup> min)	$t_{1/2}$ (min)
Brain	0.95 ± 0.15	3.4 ± 0.3	43 ± 3	6.5 ± 0.9
Heart	0.72 ± 0.15	12 ± 1	75 ± 4	2.1 ± 0.7
Lung	0.61 ± 0.15	5.9 ± 1.4	47 ± 4	1.4 ± 0.6
Gallbladder	77 ± 13	44 ± 3	2400 ± 100	-
Urinary bladder	89 ± 1	14 ± 4	780 ± 210	-
Intestine	90 ± 0	5.6 ± 0.4	390 ± 50	-
Liver	12 ± 5	7.1 ± 0.5	370 ± 60	33 ± 12
Kidneys	1.1 ± 0.2	5.9 ± 0.9	150 ± 10	21 ± 5

Abbreviations: AUC, area under the curve;  $C_{\max}$ , peak concentration; PET, positron emission tomography;  $t_{1/2}$ , half-life;  $T_{\max}$ , time to reach the  $C_{\max}$ .

nonspecific binding in all brain areas, including those without target protein, and a rapid washout in 2–30 min in healthy mice.<sup>[38]</sup>

Both dynamic images and time–activity curves support the brain penetration ability of [<sup>18</sup>F]2a. Based on PET images in mice, we expect that [<sup>18</sup>F]2a may show high in vivo stability. The skull radio uptake, which originated in dissociated free <sup>18</sup>F from [<sup>18</sup>F]2a, was not observed in the PET imaging within 90 min. The feature is according to analytical evaluation that showed high stability of 2a in mice brain homogenate (Supporting Information S1, Figure S8), which did not undergo apparent metabolism within 24 h.

Based on the PET signal, the radiolabeled [<sup>18</sup>F]2a proved to enter readily in the brain in few seconds. Recently, some radiolabeled BChE competitive inhibitors, built on DNPZ-like sulfonamides,<sup>[32,39]</sup> or pseudo-irreversible carbamate inhibitors have been reported and applied as potential PET tracers. These compounds retained enough potency of the parent lead compounds, also showing only a limited brain uptake, and were accumulated in internal organs such liver and kidneys. The presented radiolabeled [<sup>18</sup>F]2a proved to improve the ability to enter the brain. However, the highest uptake in relevant brain areas (3.35 ± 0.26 ID g<sup>-1</sup>) was exhibited at 0.95 ± 0.15 min postinjection, followed by a rapid clearance ( $t_{1/2}$  = 6.50 ± 0.93 min), which suggests that [<sup>18</sup>F]2a can cross BBB, without permanent accumulation in the brain. In particular, [<sup>18</sup>F]2a showed higher uptake in the cortex, striatum, and thalamus brain regions. The regional distribution of [<sup>18</sup>F]2a showed slightly higher initial uptake in the striatum ( $C_{\max}$  = 3.28 ± 0.13% ID g<sup>-1</sup>), HIPP ( $C_{\max}$  = 3.20 ± 0.16% ID g<sup>-1</sup>), thalamus ( $C_{\max}$  = 3.57 ± 0.17% ID g<sup>-1</sup>), and cerebellum ( $C_{\max}$  = 3.18 ± 0.15% ID g<sup>-1</sup>) than the cortex ( $C_{\max}$  = 2.73 ± 0.06% ID g<sup>-1</sup>) and brain stem ( $C_{\max}$  = 2.87 ± 0.24% ID g<sup>-1</sup>). As further illustrated by data in Table 3, a high concentration of [<sup>18</sup>F]2a in heart ( $C_{\max}$  = 11.63 ± 1.26% ID g<sup>-1</sup> at 0.72 ± 0.15 min) and lung ( $C_{\max}$  = 5.90 ± 1.39% ID g<sup>-1</sup> at 0.61 ± 0.15 min) was observed in early time of imaging, suggesting that systemic circulation contributed to the whole-body distribution, whereas the pulmonary BChE expression can explain accumulation in lung.

The gallbladder showed the greatest accumulation, as expressed by area under the curve in %ID g<sup>-1</sup> min, followed by the urinary bladder, intestine, liver, kidney, heart, lung, and brain. The substantial accumulation in the gallbladder, intestine, and liver implies that [<sup>18</sup>F] 2a may be excreted via the hepatobiliary route of excretion with a greater fraction than renal excretion.

### 3 | CONCLUSIONS

In the context of our medicinal chemistry program on small molecules as MTDLs in AD dementias, we recently discovered potent BChE-selective inhibitors built up on the THAI scaffold and disclosed the 6-phenethyl derivative 1 and its 9-F congener 2a, which displayed in vitro low neuro- and organotoxicity, nanomolar inhibition potency against human BChE, and protective effects against NMDA-induced neurotoxicity. To progress in featuring its neuropharmacological profile and suitability as an anti-AD molecule, we determined further biochemical and biophysical parameters and carried out a whole-body distribution study in healthy mice of the newly synthesized labeled analog [<sup>18</sup>F]2a. The PET imaging study proved the ability of [<sup>18</sup>F]2a to cross the BBB, appearing in the brain within 1 min after intravenous administration, followed by rapid washout, a behavior comparable with those of general brain-targeted radiotracers in healthy subjects,<sup>[40]</sup> and suggest that future studies should aim to assess [<sup>18</sup>F]2a as a potential BChE target radioligand in AD animal models.

Ex vivo neuropharmacological experiments in mice revealed diverse effects on neurotransmitters in cortical and HIPP areas 30 min after i.p. administration of 2a (20 mg kg<sup>-1</sup>). An increased level of 5-HT was observed in cortical brain areas, whereas increased NA and a reduced DA concentration appeared in HIPP. These changes in neurochemical transmission contribute to conceiving the potential of multimodal bioactive profile of 2a in neurodegenerative diseases, considering that a 5-HT level increase could contribute to enhancing the clearance of Aβ protein, whereas restoring the NA/DA balance could help in regulating cognitive and behavioral functions. In this light, screening of 2a in animal models of AD will be the logical prosecution of this work, which may provide a supporting proof of its effectiveness in the treatment of AD-related disorders.

### 4 | EXPERIMENTAL

#### 4.1 | Chemistry

##### 4.1.1 | General

Starting materials and all reagents and solvents were purchased from Sigma-Aldrich and Alfa Aesar, and were used without further purification. All reaction was monitored by precoated plates (silica gel 60F254; Merck). Melting points were determined by using the capillary method on a Stuart Scientific SMP3 electrothermal



apparatus and were uncorrected. Gas-chromatograph coupled with mass spectrometer were recorded on a JMS-700 (JEOL) and 6890 Series (Agilent). Final compound purities were assessed by elemental analyses (C, H, N), performed on a Euro EA3000 analyzer (Eurovector) by the Analytical Laboratory Service of the Department of Pharmacy-Drug Sciences of the University of Bari (Italy), and the results agreed to within  $\pm 0.4\%$  of theoretical values. Mass spectra were obtained by Agilent 1100 Series LC-MSD Trap System VL, equipped with an electrospray ionization source (ESI) (Agilent Technologies Italia S.p.A.). The high-resolution molecular masses of test compounds were assessed by Agilent 6530 Accurate Mass Q-TOF spectrometer (Agilent Technologies Italia). Infrared spectra (KBr disks) were recorded on a PerkinElmer Spectrum One Fourier transform infrared (FT-IR) spectrophotometer (PerkinElmer Ltd.), and the most significant absorption bands are listed. Proton nuclear magnetic resonance ( $^1\text{H}$  NMR) spectra were recorded at 300 MHz on a Varian Mercury 300 instrument. Carbon-13 NMR ( $^{13}\text{C}$  NMR) spectra were recorded at 500 MHz on a Varian instrument. Chemical shift data are expressed in  $\delta$  and the coupling constants  $J$  are in hertz (Hz); the following abbreviations are used for multiplicity: s, singlet; d, doublet; dd, doublet-doublet; td, triplet of doublets; t, triplet; q, quartet; m, multiplet. Signals due to NH and OH protons were located by deuterium exchange with  $\text{D}_2\text{O}$ . Chromatographic separations were performed on silica gel 60 for column chromatography (Merck 70-230 mesh).

In radiochemistry,  $\text{H}_2^{18}\text{O}$  was purchased from Taiyo Nippon Sanso Corporation.  $^{18}\text{F}$ Fluoride was produced by  $^{18}\text{O}(\text{p},\text{n})^{18}\text{F}$  reaction through proton irradiation using a cyclotron. Radio-TLC was detected by an AR-2000 radio-TLC imaging scanner (Bioscan Inc.). All radioactivity counting was analyzed by a VDC-505 (Comer) activity calibrator from Veenstra Instruments. PET imaging of mice was performed on a NanoPET/CT (Mediso).

#### 4.1.2 | General procedure for the synthesis of the 6-(2-phenylethyl)-3,4,5,6-tetrahydroazepino[4,3-*b*]indol-1(2*H*)-one derivatives (**2a-c**)

All compounds were obtained by following the reactions reported in Scheme 1. The synthesis of compound **2a** was reported as an example. Complete descriptions of the intermediates for the synthesis of compounds **2b** and **2c** were reported in the Supplementary Information. The InChI codes of compounds **2a-c**, together with some biological activity data, are also provided as Supporting Information.

**6-Fluoro-1,2,3,9-tetrahydro-4*H*-carbazol-4-one (4a):** Compound **4a** has been prepared as previously reported, with slight modifications.<sup>[18,19]</sup> To the aqueous solution of 1,3-cyclohexanedione (500 mg, 4.55 mmol) in 100 mL of water, 4-fluorophenylhydrazine hydrochloride (1.0 g, 4.55 mmol) was added portionwise and then the suspension mixture was stirred overnight (15 h) at room temperature. The precipitate was isolated by filtration, washed with 100 mL of water, and dried to obtain 510 mg (yield 52%) of 4-fluoro phenylhydrazone

(melting point [m.p.] 259–261°C). Without further purification due to low stability, the hydrazone intermediate was refluxed in 20 mL of TFA for 36 h. After cooling, the solvent was removed, and the residue was triturated with ice-cold water. The precipitate was collected by filtration and compound **4a** was isolated. Yield: 70% (675 mg). Dark brown solid. FT-IR ( $\nu_{\text{max}}$ ,  $\text{cm}^{-1}$ ) 3114, 2955, 1724, 1614, 1583, 1470, 1204, 1176, 1133, 1012, 915, 864, 808, 791.  $^1\text{H}$  NMR (300 MHz,  $\text{CDCl}_3$ )  $\delta_{\text{H}}$  ppm: 8.22 (s, 1H), 7.96 (d,  $J = 9.0$  Hz, 1H), 7.01 (t,  $J = 9.0$  Hz, 1H), 6.90–6.82 (m, 1H), 2.42 (t,  $J = 6.5$  Hz, 2H), 2.25 (t,  $J = 6.5$  Hz, 2H), 1.95 (quintet,  $J = 6.5$  Hz, 2H).

**6-Fluoro-1,2,3,9-tetrahydro-4*H*-carbazol-4-one oxime (5a):** The oxime derivative **5a** was synthesized starting from compound **4a**.<sup>[18]</sup> Sodium acetate (1.33 g, 16.2 mmol) and hydroxylamine hydrochloride (2.00 g, 28 mmol) were added to **4a** (1.90 g, 9.4 mmol) in 30 mL of ethanol (EtOH)-water (2/1 (v/v)) hydroalcoholic solution and the mixture was refluxed 24 h under nitrogen atmosphere. After cooling, the solvent was removed and the residue was suspended in 150 mL of water and triturated, until precipitation of the desired oxime product as dark gray solid, which was collected by filtration and recrystallized from EtOH and water. Yield: 80% (1.66 g). Dark brown solid. M.p. 278–279°C. FT-IR ( $\nu_{\text{max}}$ ,  $\text{cm}^{-1}$ ) 3296, 2950, 1708, 1627, 1580, 1483, 1242, 1138, 925, 896, 804, 780, 724.  $^1\text{H}$  NMR (300 MHz,  $\text{DMSO}-d_6$ )  $\delta_{\text{H}}$  ppm: 11.33 (s, 1H), 10.29 (s, 1H), 7.50 (dd,  $J_1 = 9.0$  Hz,  $J_2 = 2.0$  Hz, 1H), 7.30–7.25 (m, 1H), 6.89 (dd,  $J_1 = 8.0$  Hz,  $J_2 = 2.5$  Hz, 1H), 2.77 (t,  $J = 6.5$  Hz, 2H), 2.64 (d,  $J = 6.5$  Hz, 2H), 1.88 (quint,  $J = 6.5$  Hz, 2H).

**9-Fluoro-2,3,4,5-tetrahydroazepino[4,3-*b*]indol-1(2*H*)-one (6a):** The oxime derivative **5a** (2.5 g, 12.5 mmol) was added portionwise to preheated (110°C) 25 g of PPA under vigorous stirring. The mixture was stirred 30 min at this temperature before being poured in 100 g of ice, and triturated until complete dissolution of PPA. The obtained gray precipitate was collected by filtration under reduced pressure, washed with 100 mL of water, 10 mL of 5% diluted ammonia, and further 100 mL of water. The solid was suspended in 50 mL of MeOH and refluxed for 1 h after the addition of 500 mg of vegetal carbon. After cooling, the suspension was filtered on a Celite pad and concentrated under reduced pressure to furnish **6a**. Yield: 56% (0.72 g). Dark green solid. M.p. 274–276°C. FT-IR ( $\nu_{\text{max}}$ ,  $\text{cm}^{-1}$ ) 3222, 2922, 1618, 1487, 1452, 1128, 1099, 876, 801, 779.  $^1\text{H}$  NMR (300 MHz,  $\text{CDCl}_3$ )  $\delta_{\text{H}}$  ppm: 8.22 (s br, 1H), 8.10 (d,  $J = 9.0$  Hz, 1H), 7.18 (q,  $J = 9.0$  Hz, 1H), 6.94 (t,  $J = 9.0$ , 1H), 5.90 (s br, 1H), 3.41 (q,  $J = 6.5$  Hz, 2H), 3.16 (t,  $J = 6.5$  Hz, 2H), 2.20–2.10 (m, 2H).

**9-Fluoro-6-(2-phenylethyl)-2,3,4,5-tetrahydroazepino[4,3-*b*]indol-1(2*H*)-one (2a):** In a 50 mL round bottom flask, TBAB (0.445 g, 1.38 mmol), phenethyl bromide (0.3 mL, 2.28 mmol), and 5.0 mL of 25% w/w NaOH solution were added to a solution of **5a** (0.250 g, 1.14 mmol) in 15 mL of dry dichloromethane (DCM). The mixture was stirred at room temperature for 48 h and then diluted with 20 mL of DCM and 20 mL of water. The collected organic phase was washed twice with 20 mL of brine, dried over  $\text{Na}_2\text{SO}_4$ , filtered, and concentrated under reduced pressure. The residue was purified by chromatography on silica gel, eluting with ethyl acetate to afford **2a**. White solid. Yield 51% (0.120 g). FT-IR ( $\nu_{\text{max}}$ ,  $\text{cm}^{-1}$ ) 3437, 3027, 2921, 1634, 1523, 1470, 1384, 1132,

886, 787, 667.  $^1\text{H}$  NMR (300 MHz, DMSO- $d_6$ )  $\delta_{\text{H}}$  ppm: 7.93 (d,  $J = 8.0$  Hz, 1H), 7.60–7.40 (m, 2H), 7.25–7.15 (m, 3H), 7.08 (d,  $J = 7.0$  Hz, 2H), 6.98 (t,  $J = 7.5$  Hz, 1H), 4.33 (t,  $J = 7.0$  Hz, 2H), 3.15–3.05 (m, 2H), 2.95 (t,  $J = 7.5$  Hz, 2H), 2.76 (t,  $J = 6.5$  Hz, 2H), 1.90–1.80 (m, 2H);  $^{13}\text{C}$  NMR (126 MHz,  $\text{CDCl}_3$ )  $\delta_{\text{C}}$  ppm: 26.3, 27.4, 35.6, 41.5, 45.3, 108.2, 109.3, 110.7, 127.0, 128.8 (2C), 128.9 (2C), 132.2, 137.8, 143.7, 159.1, 168.7. HR MS (ESI)  $m/z$  calcd for  $[\text{C}_{20}\text{H}_{20}\text{FN}_2\text{O}]^+$  323.1554, found, 323.1552. Anal. calcd for  $\text{C}_{20}\text{H}_{19}\text{FN}_2\text{O}$ : C, 74.51; H, 5.94; N, 8.69%; found: C, 74.44; H, 6.00; N, 8.65%.

9-Bromo-6-(2-phenylethyl)-2,3,4,5-tetrahydroazepino[4,3-*b*]indol-1(2*H*)-one (**2b**): Compound **2b** was synthesized according to the method described for compound **2a**, using derivative **6b** (250 mg, 0.90 mmol) and phenethyl bromide (0.3 mL, 2.28 mmol). Yield 50% (120 mg). Brown solid. FT-IR ( $\nu_{\text{max}}$ ,  $\text{cm}^{-1}$ ) 3262, 1631, 1525, 780, 752, 698.  $^1\text{H}$  NMR (300 MHz,  $\text{CDCl}_3$ )  $\delta_{\text{H}}$  ppm: 8.63 (d,  $J = 1.8$  Hz, 1H), 7.33 (dd,  $J = 8.5$ , 2.0 Hz, 1H), 7.25–7.18 (m, 3H), 7.14-(d,  $J = 8.5$  Hz, 1H), 6.94–6.93 (m, 1H), 6.22 (t, br,  $J = 4.5$  Hz, 1H), 4.25 (t,  $J = 7.0$  Hz, 2H), 3.25–3.15 (m, 2H), 3.02 (t,  $J = 7.0$  Hz, 2H), 2.52 (t,  $J = 7.0$  Hz, 2H), 1.91 (dd,  $J = 8.2$ , 6.5 Hz, 2H);  $^{13}\text{C}$  NMR (126 MHz,  $\text{CDCl}_3$ )  $\delta_{\text{C}}$  ppm: 26.3, 27.3, 35.60, 41.6, 45.8, 104.0, 109.3, 112.0, 126.5, 128.6(2C), 128.8, 128.90 (2C), 130.8, 137.9, 141.9, 155.8, 166.4. HR MS (ESI)  $m/z$  calcd for  $[\text{C}_{20}\text{H}_{20}\text{BrN}_2\text{O}]^+$  383.0754, found, 383.0762. Anal. calcd for  $\text{C}_{20}\text{H}_{19}\text{BrN}_2\text{O}$ : C, 62.67; H, 5.00; N, 7.31%; found: C, 62.73; H, 5.05; N, 7.45%.

9-Methoxy-6-(2-phenylethyl)-2,3,4,5-tetrahydroazepino[4,3-*b*]indol-1(2*H*)-one (**2c**): Compound **2c** was synthesized according to the method described for compound **2a**, intermediate **6c** (250 g, 1.08 mmol) and phenethyl bromide (0.42 mL, 3.26 mmol). Brown solid. Yield 61% (0.120 g). FT-IR ( $\nu_{\text{max}}$ ,  $\text{cm}^{-1}$ ) 3412, 3272, 2931, 1632, 1473, 1279, 1151, 746, 701.  $^1\text{H}$  NMR (300 MHz,  $\text{CDCl}_3$ )  $\delta_{\text{H}}$  ppm: 8.01 (d,  $J = 2.4$  Hz, 1H), 7.24–7.19 (m, 4H), 6.95–6.89 (m, 3H), 6.01 (s br, 1H), 4.26 (t,  $J = 6.9$  Hz, 2H), 3.90 (s, 3H), 3.21–3.14 (m, 3H), 3.04 (t,  $J = 6.7$  Hz, 2H), 2.54 (t,  $J = 6.7$  Hz, 2H), 1.96–1.89 (m, 2H).  $^{13}\text{C}$  NMR (126 MHz,  $\text{CDCl}_3$ )  $\delta_{\text{C}}$  ppm: 26.3, 27.2, 35.7, 41.6, 45.2, 55.8, 104.1, 109.6, 113.0, 126.9, 128.6 (2C), 128.8, 128.9, 128.90 (2C), 130.7, 138.0, 142.8, 155.7, 169.2. HR MS (ESI)  $m/z$  calcd for  $[\text{C}_{21}\text{H}_{23}\text{N}_2\text{O}_2]^+$  335.1754, found, 335.1769. Anal. calcd for  $\text{C}_{21}\text{H}_{22}\text{N}_2\text{O}_2$ : C, 75.42; H, 6.63; N, 8.38%; found: C, 75.52; H, 6.60; N, 8.45%.

#### 4.1.3 | Preparation of 6-phenethyl-9-(4,4,5,5-tetramethyl-1,3,2-dioxaborolan-2-yl)-2,3,4,5-tetrahydroazepino[4,3-*b*]indol-1(2*H*)-one (**7**)

The bromine-substituted derivative **2b** (184 mg, 0.48 mmol), [1,1'-bis(diphenylphosphino)ferrocene]palladium(II) dichloride (41 mg, 0.05 mmol), potassium acetate (141 mg, 1.4 mmol), and bis(pinacolato)diboron (134 mg, 0.53 mmol) were dissolved in DMF (10 mL) and then stirred at 80°C for 5 h under argon atmosphere. After cooling, the reaction mixture was diluted by DCM (10 mL) and filtered through a Celite layer. The filtrate was washed with water (3 × 10 mL), dried over anhydrous  $\text{Na}_2\text{SO}_4$  and then concentrated under reduced pressure. The crude

product was finally purified by silica gel column chromatography using 50% ethyl acetate-hexane (v/v) as the eluent to give compound **7**. White solid. Yield 31% (64 mg). M.p. 128–131°C.  $^1\text{H}$  NMR (300 MHz, DMSO- $d_6$ )  $\delta_{\text{H}}$  ppm: 8.68 (s, 1H), 7.58–7.53 (m, 1H), 7.50–7.46 (m, 2H), 7.30–7.20 (m, 3H), 7.10–7.04 (m, 2H), 4.35 (t,  $J = 6.8$  Hz, 2H), 3.15–2.95 (m, 2H), 2.98 (t,  $J = 6.8$  Hz, 2H), 2.76 (t,  $J = 6.8$  Hz, 2H), 1.90–1.80 (m, 2H), 1.31 (s, 12H);  $^{13}\text{C}$  NMR (100 MHz, DMSO- $d_6$ )  $\delta_{\text{H}}$  ppm: 167.2, 142.8, 138.3, 137.6, 129.6, 129.0, 128.4, 127.7, 127.5, 126.6, 108.9, 107.0, 83.2, 44.4, 34.9, 26.8, 26.4, 24.8. HR MS (FAB)  $m/z$  calcd for  $[\text{C}_{26}\text{H}_{32}\text{BN}_2\text{O}_3]^+$  431.2506, found 431.2504.

#### 4.1.4 | Preparation and purification of 9- $^{18}\text{F}$ fluoro-6-phenethyl-2,3,4,5-tetrahydroazepino[4,3-*b*]indol-1(2*H*)-one ( $^{18}\text{F}$ **2a**)

Radiosynthesis of  $^{18}\text{F}$ **2a** was conducted according to our previous report.<sup>[20,21]</sup> Briefly, a volume of 100  $\mu\text{L}$  of  $^{18}\text{O}$ -enriched water containing  $^{18}\text{F}$  (370 MBq) was diluted with deionized water (900  $\mu\text{L}$ ) and passed through a Chromafix-HCO3 cartridge. Then,  $^{18}\text{F}$  ion on the cartridge was eluted by a mixture of 18-Crown-6 (0.18 mg, 0.7  $\mu\text{mol}$ ) dissolved in 1 mL of methanol, and  $\text{CsHCO}_3$  (0.10 mg, 0.5  $\mu\text{mol}$ ) in 10  $\mu\text{L}$  of water. The mixture was dried by azeotropic distillation with acetonitrile twice ( $\text{CH}_3\text{CN}$ , 2 × 0.3 mL) at 90°C under a nitrogen stream. Meanwhile, 6-phenethyl-9-(4,4,5,5-tetramethyl-1,3,2-dioxaborolan-2-yl)-3,4,5,6-tetrahydroazepino[4,3-*b*]indol-1(2*H*)-one (**7**, 2.5 mg, 5.7  $\mu\text{mol}$ ),  $\text{Cu}(\text{OTf})_2$  (1.2 mg, 3.3  $\mu\text{mol}$ ) and pyridine (8.2  $\mu\text{L}$ , 102  $\mu\text{mol}$ ) was dissolved in DMF (0.4 mL) and then added to the reaction vial containing the dried 18-Crown-6/ $^{18}\text{F}$ - $\text{Cs}^+$  complex, followed by heating at 110°C for 10 min. After the reaction, the mixture was diluted with deionized water (10 mL) and loaded into a tC18 Sep-Pak cartridge. The mixture loaded on the tC18 Sep-Pak cartridge was washed with water (10 mL) and eluted with acetonitrile (1.0 mL). Finally, the reaction mixture was purified by a semipreparative HPLC system (Waters, Xterra semipreparative C18 column, 10 × 250 mm, 10  $\mu\text{m}$ ; 40%  $\text{CH}_3\text{CN}$ -water containing 0.1% formic acid;  $\lambda = 254$  nm, flow rate = 3.0  $\text{ml min}^{-1}$ ) equipped with an ultraviolet (UV) detector and a  $\gamma$ -ray detector. The radiochemical purity of each  $^{18}\text{F}$ **2a** fraction, collected from the HPLC, was determined by analytical HPLC (stationary phase: Waters, Xterra RP-18 C18 column, 4.6 × 250 mm, 5  $\mu\text{m}$ ; mobile phase: 65%  $\text{CH}_3\text{CN}$ -35% water v/v; flow rate = 1.0  $\text{mL min}^{-1}$ ) equipped with a UV detector ( $\lambda = 254$  nm) and a  $\gamma$ -ray detector ( $t_{\text{R}} = 5.8$  min for  $^{18}\text{F}$ **2a**). To determine the molar activity, calibration curves were obtained by measuring peak areas from four known concentrations of the authentic compound **2a** dissolved in 65%  $\text{CH}_3\text{CN}$ -35% water (v/v) HPLC solution (Supporting Information, Figure S4). The fraction of  $^{18}\text{F}$ **2a** collected from the HPLC system was diluted with water (20 mL) and exchanged for 5% EtOH-saline solution using a tC18 Sep-Pak cartridge for the further studies.

The HPLC profile of crude mixture after aromatic  $^{18}\text{F}$ -fluorination to obtain  $^{18}\text{F}$ **2a**, and the HPLC chromatograms of  $^{18}\text{F}$ **2a** coinjected with the standard **2a** have been reported in Supporting Information S1, Figures S1 and S2, respectively.

## 4.2 | Physicochemical characterization

### 4.2.1 | Aqueous solubility measurements

The aqueous solubility at equilibrium of compounds **2** was determined at pH 7.4 in a 0.05 M PB (containing 0.15 M KCl as an ionic strength regulator) prepared in deionized water, as previously reported.<sup>[18,41]</sup> An excess of each compound (2–5 mg) was suspended in 1 mL of buffered solution. The obtained suspension was shaken for 1 h at 25°C and then maintained 15 min at the same temperature without shaking to ensure reaching of the solubility equilibrium. The supernatant was drawn off, filtered (Millipore; 0.45 µm), and analyzed by RP-HPLC on Agilent 1290 HPLC/UPLC apparatus with UV-Vis diode-array. Analyses were performed on a Phenomenex Gemini C18 column (2.1 µm, 150 mm × 2.6 mm i.d.), by using MeOH (70% v/v) and deionized MilliQ grade water (30% v/v) as mobile phase. The flow rate was set at 0.2 mL/min, and UV detection was set at λ 254 nm. Calibration curves were obtained by measuring peak areas, eluted under the same conditions, for at least seven known concentrations of methanol solution.

### 4.2.2 | Log *D* measurement of [<sup>18</sup>F]**2a**

[<sup>18</sup>F]**2a** (7.4 MBq) in 5% EtOH-saline (10 µL) was added to a mixture of PBS (5.0 mL, 0.15 M, pH 7.4) and *n*-octanol (5 mL) in a test tube (*n* = 5). After vortexing for 1 min, the tube was placed on the table at 25°C for 10 min. The radioactivity in each phase (100 µL) was measured by using a γ-counter. Log *D* was expressed as the logarithm of the ratio of the counts from *n*-octanol versus that of PBS.

### 4.2.3 | Stability of [<sup>18</sup>F]**2a** in human serum

To assess the *in vitro* stability of radioligand, [<sup>18</sup>F]**2a** in 5% EtOH-saline (3.7 MBq, 0.2 mL) was incubated with human serum (1.8 mL) from a healthy volunteer for 180 min at 37°C. Aliquots (0.2 mL) were taken at 0, 30, 60, 90, and 180 min and mixed with CH<sub>3</sub>CN (0.2 mL), and then centrifuged at 3500 rpm for 5 min. The resulting supernatants were analyzed by a radio-TLC scanner using the developing solvent (10% methanol-DCM, R<sub>f</sub> = 0.5 for [<sup>18</sup>F]**2a**).

## 4.3 | Biological evaluation

### 4.3.1 | Cholinesterases' inhibition assay

The inhibitory activity of newly synthesized compounds toward horse and human BChE, and either ee AChE (Sigma-Aldrich), was assessed by following Ellman's method, with slight modifications, on a 96-well plate system.<sup>[42,43]</sup> The BChE activity was determined in a reaction mixture containing 20 µL of a BChE solution (1.8 U/mL in 0.1 M, pH 8.0 PB), 20 µL of 5,5-dithio-bis-(2-nitrobenzoic) acid

(3.3 mM in 0.1 M, pH 7.0 PB, containing 0.1 mM NaHCO<sub>3</sub>), 20 µL of a solution of the test compound (ranging from 1 × 10<sup>-4</sup> to 1 × 10<sup>-9</sup> M in 0.1 M, pH 8.0 PB), and 120 µL of pH 8.0 PB. After 20 min incubation at 25°C, the substrate butyrylthiocholine iodide (20 µL, 0.05 mM solution in PB) was added, and its hydrolysis rates were monitored for 10 min at λ 412 nm. The concentration of the compound, which produced 50% inhibition of the BChE activity (IC<sub>50</sub>), was calculated by nonlinear regression of the response/concentration (log) curve, by using Prisma GraphPad software (ver. 5.01), thus plotting the initial rate values. The AChE inhibitory activity was similarly determined by using a solution of AChE (0.9 U/mL in 0.1 M, pH 8.0 PB), and acetylthiocholine iodide (0.05 mM) as enzyme and substrate, respectively. The inhibition data are reported as means of IC<sub>50</sub> values determined at least in three independent measurements.

### 4.3.2 | *In vivo* PET imaging studies

Before PET imaging, the healthy male ICR mice (7 weeks old, 20–25 g, *n* = 3) were anesthetized with 2% isoflurane, then intravenously injected with approximately 7.4 MBq of [<sup>18</sup>F]**2a** dissolved in 5% EtOH-saline (100 µL). Ninety-minute dynamic list-mode acquisition started immediately after the intravenous administration of [<sup>18</sup>F]**2a**. The molar activity of [<sup>18</sup>F]**2a** solution at the time of injection was 109.15 GBq/µmol. The data were reconstructed using three-dimensional ordered subset expectation maximization methods with CT-based attenuation correction, binned into 54 frames of 12 frames × 10 s, 16 frames × 30 s, 8 × 1 min, 18 × 4 min. The data were analyzed using PMOD software version 3.6 and expressed as the percentage of the injected dose per gram of tissue (%ID g<sup>-1</sup>).

### 4.3.3 | Neurochemical assays

Experiments were performed on 10-week-old male C57BL/6 mice (Envigo). Animals were constantly maintained under controlled conditions, with a room temperature of 22 ± 1°C, relative humidity of 55 ± 5%, and a light/dark cycle of 12 h (light on from 7:00 a.m. to 7:00 p.m.). Mice were group-housed, and food and water were provided *ad libitum*. All experimental procedures involving animals were conducted in conformity with the institutional guidelines of the Italian Ministry of Health (D.L. 26/2014), the Guide for the Care and Use of Mammals in Neuroscience and Behavioral Research (National Research Council 2004), the Directive 2010/63/EU of the European Parliament, and of the Council of 22 September 2010, on the protection of animals used for scientific purposes, as well as the ARRIVE guidelines. The Italian Ministry of Health approved our experimental protocol (protocol number: B2EF8.23). Animal welfare was daily monitored to detect any signs of animal suffering or distress during the entire experimental procedure. All efforts to reduce the number of animals used and their suffering were conducted.

#### Postmortem analysis

Mice received intraperitoneal injection of compound **2a** at 20 mg 10 mL<sup>-1</sup> kg<sup>-1</sup> (or vehicle sunflower oil). Thirty minutes after drug administration, animals were euthanized, and brains were dissected by using a chilled rat brain matrix (World Precision Instruments Inc.), as previously described.<sup>[30]</sup> The PFC and the HIPP were weighed, frozen in liquid nitrogen, and stored at -80°C until ex vivo HPLC quantifications were performed.

#### Neurotransmitters RP-HPLC quantifications

Neurochemical analyses were performed by using HPLC. PFC and HIPP samples were homogenized in 10 volumes (w/v) of 0.1 N perchloric acid, stored on ice for 30 min, and then centrifuged at 10,000g for 10 min at 4°C, as previously described.<sup>[44,45]</sup> Supernatants were then collected and HPLC analyses were carried out. NA, DA, and 5-HT concentrations were determined by using an LC18 reverse phase column (Kinetex, 150 mm × 4.2 mm, ODS 5 μm; Phenomenex). An electrochemical detector with a thin-layer amperometric cell (Ultimate 3000RS-ECD, Dionex; Thermo Scientific) at a working potential of 0.400 V was used. The flow rate was maintained at 0.7 mL min<sup>-1</sup> by an isocratic pump (Shimadzu LC-10 AD). The mobile phase consisted of an aqueous solution of 75 mM NaH<sub>2</sub>PO<sub>4</sub>, 1.7 mM octane sulfonic acid, 0.3 mM EDTA, and acetonitrile 10%, buffered at pH 3. Chemicals and reagents were purchased from Sigma-Aldrich. Chromeleon software (version 6.80; Thermo Scientific Dionex) was used for data analyses. Neurotransmitter concentrations were expressed as fmol mg<sup>-1</sup> of tissue.

## 4.4 | SPR assays

### 4.4.1 | Kinetics of interactions with BChE

Affinity studies by using SPR were performed on a Pioneer SensiQ SPR instrument (Pall FortèBio, Alfatest; Cinisello Balsamo). BChE was first immobilized on a COOH V sensor chip (Pall FortèBio) surface by amine coupling, resulting in a stable biosensor. After purification and conditioning of the new sensor chip by flowing HCl, NaOH, and SDS, the surface underwent equilibration by flowing 10 mM PB (pH 8) at a flow rate of 20 μL min<sup>-1</sup>. The carboxymethylated dextran layer on the sensor chip surface was then activated within 10 min by injection of an employing *N*-(3-dimethylaminopropyl)-*N*-ethylcarbodiimide (EDC)/*N*-hydroxysuccinimide (NHS) solution. Equine BChE (52 U mL<sup>-1</sup>) was dissolved in 10 mM sodium acetate (pH 4.5) and coupled over the surface by three different and sequential injections of enzyme solutions for 10 min at a flow rate of 25 μL min<sup>-1</sup>. After immobilization of the ligand, the unreacted NHS esters were blocked by washing overnight (throughout 18 h) with 0.05 M Tris solution (pH 8), containing 0.1 M NaCl, at a flow rate of 20 μL min<sup>-1</sup>. Stability of the biosensors was tested by repeating regeneration cycles with a 3 M NaCl solution injection (5 μL, flow rate = 50 μL min<sup>-1</sup>), without any significant change in the surface

responses. Immobilization of the BChE was obtained in flow cells 1 and 3 (unmodified dextran surface in flow cell 2 was used as a reference). A final apparent level of about 7000 RU was achieved. The assay protocols were as follows: assay solutions of tested compounds were prepared by dissolving 10 mM DMSO solutions in 10 mM PB (pH 8) up to a final 2% DMSO concentration, as in the running buffer. After 10 leadoff blanks, the assay solutions were injected over a BChE functionalized surface at a flow rate of 25 μL min<sup>-1</sup> for 4 min, to avoid any limitation by mass transfer. On completion of injection, the running buffer flowed over the surface to allow a dissociation time of 180 s. All binding experiments were carried out at 25°C, without regeneration cycles. Each interaction was at least in triplicate and analyzed by using QDAT software (nonlinear regression analysis of 1:1 stoichiometric reversible binding model), and double referencing.

### 4.4.2 | Kinetics of interactions with HSA

The HSA functionalized surface on COOH V sensor chip (Pall FortèBio) was prepared by using amine coupling, by (EDC/NHS), and HSA (Sigma-Aldrich A3782). Briefly, HSA aqueous stock solution was diluted at a final concentration of 50 μg mL<sup>-1</sup> in 10 mM sodium acetate buffer (pH 5.0), and immobilization in flow cells 1 and 3 (unmodified dextran surface in flow cell 2 was used as a reference) at a final apparent level of about 5000 RU was achieved as follows: injection of EDC/NHS (freshly mixed 0.4 M EDC and 0.1 M NHS) 1:1 v/v at a flow rate of 25 μL min<sup>-1</sup> for 4 min; injection of HSA solution at a flow rate of 25 μL min<sup>-1</sup> for 8 min; capping on unreacted activated carboxyl groups by injection of 1 M ethanolamine solution (pH 9) at a flow rate of 25 μL min<sup>-1</sup> for 8 min. The functionalized surface was then treated with repeated injections of 4 M NaCl, and conditioned overnight before use with PBS (pH 7.4) (10 mM NaH<sub>2</sub>PO<sub>4</sub> and 150 mM NaCl) as the running buffer. Each cycle for binding assay to HSA was carried out in PBS-2% DMSO, without regeneration necessary, and consisted of run buffer injection (60 s), injection of analyte single concentration for 120 s (ranging from 1 to 200 μM) at a flow rate of 20 μL min<sup>-1</sup>, and a dissociation phase for 150 s (flow rate = 20 μL min<sup>-1</sup>). Each interaction was at least in triplicate and analyzed by using QDAT software (nonlinear regression analysis of 1:1 stoichiometric reversible binding model), and double referencing.

#### ACKNOWLEDGMENTS

This work was supported in part by the National Research Foundation of Korea (NRF) grant funded by the Korean government (MEST) (2021R1A2C2003301). R. P. was supported by funds of the Program of Regione Puglia "Research for Innovation REFIN" (POR PUGLIA FESR-FSE 2014/2020). M. d. C., R. P., M. C., and C. D. A. acknowledge the financial support of the Italian Ministry of Education, Universities and Research (PRIN, Grant 201744BN5T\_004).

#### CONFLICTS OF INTEREST STATEMENT

The authors declare no conflicts of interest.

## ORCID

Modesto de Candia  <http://orcid.org/0000-0002-4570-1981>

## REFERENCES

- [1] <https://www.alzint.org/resource/world-alzheimer-report-2022/> in the Alzheimer's Disease International Organization website.
- [2] W. J. Geldenhuys, A. S. Darvesh, *Expert. Rev. Neurother.* **2015**, *15*, 3.
- [3] F. Chiti, C. M. Dobson, *Annu. Rev. Biochem.* **2017**, *86*, 27.
- [4] D. Puzzo, J. Fiorito, R. Purgatorio, W. Gulisano, A. Palmeri, O. Arancio, R. Nicholls, in *Genes, Environment and Alzheimer's Disease* (Eds: O. Lazarov, G. Tesco), Academic Press, New York **2016**, p. 1.
- [5] R. Wang, P. H. Reddy, *J. Alzheimer's Dis.* **2017**, *57*, 1041.
- [6] A. Silver, *The Biology of Cholinesterases*, North-Holland Pub. Co.; American Elsevier Pub. Co., Amsterdam; NewYork **1974**.
- [7] Z. Y. Ha, S. Mathew, K. Y. Yeong, *Curr. Protein Pept. Sci.* **2020**, *21*, 99.
- [8] M. Roberson, *Brain Res. Rev.* **1997**, *25*, 50.
- [9] P. Davies, *Lancet* **1976**, *308*, 1403.
- [10] E. K. Perry, P. H. Gibson, G. Blessed, R. H. Perry, B. E. Tomlinson, *J. Neurol. Sci.* **1977**, *34*, 247.
- [11] N. H. Greig, T. Utsuki, D. K. Ingram, Y. Wang, G. Pepeu, C. Scali, Q. S. Yu, J. Mamczarz, H. W. Holloway, T. Giordano, D. Chen, K. Furukawa, K. Sambamurti, A. Brossi, D. K. Lahiri, *Proc. Natl Acad. Sci. USA* **2005**, *102*, 17213.
- [12] S. Darvesh, M. K. Cash, G. A. Reid, E. Martin, A. Mitnitski, C. Geula, *J. Neuropathol. Exp. Neurol.* **2012**, *71*, 2.
- [13] H. Xu, S. Garcia-Ptacek, L. Jönsson, A. Wimo, P. Nordström, M. Eriksdotter, *Neurology* **2021**, *96*, e2220.
- [14] S. Darvesh, *Chem.-Biol. Interact.* **2013**, *203*, 354.
- [15] A. Carotti, M. de Candia, M. Catto, T. N. Borisova, A. V. Varlamov, E. Méndez-Álvarez, R. Soto-Otero, L. G. Voskressensky, C. Altomare, *Bioorg. Med. Chem.* **2006**, *14*, 7205.
- [16] M. de Candia, G. Zaetta, N. Denora, D. Tricarico, M. Majellaro, S. Cellamare, C. D. Altomare, *Eur. J. Med. Chem.* **2017**, *125*, 288.
- [17] R. Purgatorio, M. de Candia, M. Catto, A. Carrieri, L. Pisani, A. De Palma, M. Toma, O. A. Ivanova, L. G. Voskressensky, C. D. Altomare, *Eur. J. Med. Chem.* **2019**, *177*, 414.
- [18] R. Purgatorio, M. de Candia, M. Catto, M. Rullo, L. Pisani, N. Denora, A. Carrieri, A. A. Nevskaya, L. G. Voskressensky, C. D. Altomare, *ChemMedChem* **2021**, *16*, 589.
- [19] G. L. Eilman, K. D. Courtney, V. Andres, R. M. Feather-Stone, *Biochem. Pharmacol.* **1961**, *7*, 88.
- [20] M. G. Morgese, S. Schiavone, L. Trabace, *Eur. J. Pharmacol.* **2017**, *817*, 22.
- [21] S. Schiavone, P. Tucci, E. Mhillaj, M. Bove, L. Trabace, M. G. Morgese, *Progr. Neuro-Psychopharmacol. Biol. Psychiatry* **2017**, *78*, 114.
- [22] Y. I. Sheline, T. West, K. Yarasheski, R. Swarm, M. S. Jasielc, J. R. Fisher, W. D. Ficker, P. Yan, C. Xiong, C. Frederiksen, M. V. Grzelak, R. Chott, R. J. Bateman, J. C. Morris, M. A. Mintun, J. M. Lee, J. R. Cirrito, *Sci. Transl. Med.* **2014**, *6*, 236.
- [23] J. R. Cirrito, B. M. Disabato, J. L. Restivo, D. K. Verges, W. D. Goebel, A. Sathyan, D. Hayreh, G. D'Angelo, T. Benzinger, H. Yoon, J. Kim, J. C. Morris, M. A. Mintun, Y. I. Sheline, *Proc. Natl Acad. Sci. USA* **2011**, *108*, 14968.
- [24] L. Trabace, T. Cassano, A. Loverre, L. Steardo, V. Cuomo, *CNS Drug Rev.* **2002**, *8*, 53.
- [25] M. R. Marien, F. C. Colpaert, A. C. Rosenquist, *Brain Res. Rev.* **2004**, *45*, 38.
- [26] M. G. Morgese, M. Bove, M. Francavilla, S. Schiavone, S. Dimonte, A. L. Colia, M. Bevilacqua, L. Trabace, P. Tucci, *Biomolecules* **2021**, *11*, 686.
- [27] E. Galea, M. T. Heneka, C. D. Russo, D. L. Feinstein, *Cell. Mol. Neurobiol.* **2003**, *23*, 625.
- [28] S. Kalinin, V. Gavrilyuk, P. E. Polak, R. Vasser, J. Zhao, M. T. Heneka, D. L. Feinstein, *Neurobiol. Aging* **2007**, *28*, 1206.
- [29] S. Lim, D. Song, S. Jeon, Y. Kim, H. Kim, S. Lee, H. Cho, B. C. Lee, S. E. Kim, K. Kim, E. Lee, *Org. Lett.* **2018**, *20*, 7249.
- [30] F. M. Zhou, Y. Liang, J. A. Dani, *Nat. Neurosci.* **2001**, *4*, 1224.
- [31] S. Darvesh, D. L. Grantham, D. A. Hopkins, *J. Comp. Neurol.* **1998**, *393*, 374.
- [32] C. Gentzsch, X. Chen, P. Spatz, U. Kořak, D. Knez, N. Nose, S. Gobec, T. Higuchi, M. Decker, *Mol. Imaging Biol.* **2021**, *23*, 505.
- [33] L. Rejc, V. Gómez-Vallejo, A. Joya, O. Moreno, A. Egimendia, P. Castellnou, X. Ríos-Anglada, U. Cossío, Z. Baz, R. Passannante, I. Tobalina-Larrea, P. Ramos-Cabrer, A. Giralt, M. Sastre, E. Capetillo-Zarate, U. Kořak, D. Knez, S. Gobec, M. Marder, A. Martin, J. Llop, *Theranostics* **2021**, *11*, 6542.
- [34] S. H. Lee, N. Denora, V. Laquintana, G. F. Mangiardi, A. Lopodota, A. Lopalco, A. Cutrignelli, M. Franco, P. Delre, I. H. Song, H. W. Kim, S. B. Kim, H. S. Park, K. Kim, S. Y. Lee, H. Youn, B. C. Lee, S. E. Kim, *Eur. J. Nucl. Med. Mol. Imaging* **2021**, *49*, 110.
- [35] M. B. Haskali, P. D. Roselt, T. J. O'Brien, C. A. Hutton, I. Ali, L. Vivash, B. Jupp, *Molecules* **2022**, *27*, 5931.
- [36] F. Cheng, W. Li, Y. Zhou, J. Shen, Z. Wu, G. Liu, P. W. Lee, Y. Tang, *J. Chem. Inf. Model.* **2012**, *52*, 3099.
- [37] R. Waterhouse, *Mol. Imaging Biol.* **2003**, *5*, 376.
- [38] D. Brockschneider, H. Schmitt-Willich, T. Heinrich, A. Varrone, B. Gulyás, M. Toth, J. Andersson, U. Boemer, S. Krause, M. Friebe, L. Dinkelborg, C. Halldin, T. Dyrks, *J. Nucl. Med.* **2012**, *53*, 1794.
- [39] C. Gentzsch, M. Hoffmann, Y. Ohshima, N. Nose, X. Chen, T. Higuchi, M. Decker, *ChemMedChem* **2021**, *16*, 1427.
- [40] S. J. Oh, M. H. Kim, S. J. Han, K. J. Kang, I. O. Ko, Y. Kim, J.-A. Park, J. Y. Choi, K. C. Lee, D. Y. Chi, Y. J. Lee, K. M. Kim, *Mol. Pharm.* **2017**, *14*, 3114.
- [41] B. D. Belviso, R. Caliendo, M. de Candia, G. Zaetta, G. Lopopolo, F. Incampo, M. Colucci, C. D. Altomare, *J. Med. Chem.* **2014**, *57*, 8563.
- [42] R. Purgatorio, N. Gambacorta, M. de Candia, M. Catto, M. Rullo, L. Pisani, O. Nicolotti, C. D. Altomare, *Molecules* **2021**, *26*, 5208.
- [43] R. Purgatorio, N. Gambacorta, F. Samarelli, G. Lopopolo, M. de Candia, M. Catto, O. Nicolotti, C. D. Altomare, *Molecules* **2022**, *27*, 4269.
- [44] M. Morgese, P. Tucci, M. Colaianna, M. Zotti, V. Cuomo, S. Schiavone, L. Trabace, *Curr. Pharm. Des.* **2014**, *20*, 2539.
- [45] E. Mhillaj, M. G. Morgese, P. Tucci, A. Furiano, L. Luongo, M. Bove, S. Maione, V. Cuomo, S. Schiavone, L. Trabace, *Neuroscience* **2018**, *372*, 58.

## SUPPORTING INFORMATION

Additional supporting information can be found online in the Supporting Information section at the end of this article.

**How to cite this article:** S. H. Lee, R. Purgatorio, F. Samarelli, M. Catto, N. Denora, M. G. Morgese, P. Tucci, L. Trabace, H. W. Kim, H. S. Park, S. E. Kim, B. C. Lee, M. Candia, C. D. Altomare, *Arch. Pharm.* **2023**, e2300491.  
<https://doi.org/10.1002/ardp.202300491>